Albumin as a "Trojan Horse" for Polymeric Nanoconjugates Transendothelial Transport across Tumor Vasculatures for Improved Cancer Targeting

Qian Yin[1], **Li Tang**[1], **Kaimin Cai**[1], **Xujuan Yang**[2], **Lichen Yin**[1], **Yanfeng Zhang**[1], **Lawrence W. Dobrucki**[3], **William G. Helferich**[2], **Timothy M. Fan**[4], and **Jianjun Cheng**[1,3,5,6,7,8]

[1]Department of Material Sciences and Engineering, University of Illinois at Urbana-Champaign, Urbana, IL 61801, USA

[2]Department of Food Science and Human Nutrition, University of Illinois at Urbana-Champaign, Urbana, IL 61801, USA

[3]Department of Bioengineering, University of Illinois at Urbana-Champaign, Urbana, IL 61801, USA

[4]Department of Veterinary Clinical Medicine, University of Illinois at Urbana-Champaign, Urbana, IL 61801, USA

[5]Department of Chemistry, University of Illinois at Urbana-Champaign, Urbana, IL 61801, USA

[6]Beckman Institute for Advanced Science and Technology, University of Illinois at Urbana-Champaign, Urbana, IL 61801, USA

[7]Frederick Seitz Materials Research Laboratory, University of Illinois at Urbana-Champaign, Urbana, IL 61801, USA

[8]Carl R. Woese Institute for Genomic Biology, University of Illinois at Urbana-Champaign, Urbana, IL 61801, USA

Abstract

Although polymeric nanoconjugates (NCs) hold great promise for the treatment of cancer patients, its clinical utility has been hindered by lack of efficient delivery of therapeutics into targeted tumor sites. Here, we describe an albumin-functionalized polymeric NC (Alb-NC) capable of crossing the endothelium barrier through caveolae-mediated transcytosis pathway to better target cancer. The Alb-NC is prepared by nanoprecipitation of doxorubicin (Doxo) conjugates of poly(phenyl *O*-carboxyanhydrides) bearing aromatic albumin-binding domains followed by subsequent surface decoration of albumin. Administration of Alb-NCs in mice bearing MCF-7 human breast cancer xenografts with limited tumor vascular permeability resulted in markedly increased tumor accumulation and anti-tumor efficacy compared to its conventional counterpart PEGylated NCs (PEG-NCs). Alb-NC provides a simple, low-cost and broadly applicable strategy to improve the cancer targeting efficiency and therapeutic effectiveness of polymeric nanomedicine.

---

*Address correspondence to jianjunc@illinois.edu.

ASSOCIATED CONTENT

Supporting Information **Available:** This material is available free of charge via the Internet at http://pubs.acs.org.

Graphical abstract

Albumin-bound Nanoconjugates

Transendothelial transport

PET/CT 6h p.i.

Tumor accumulation
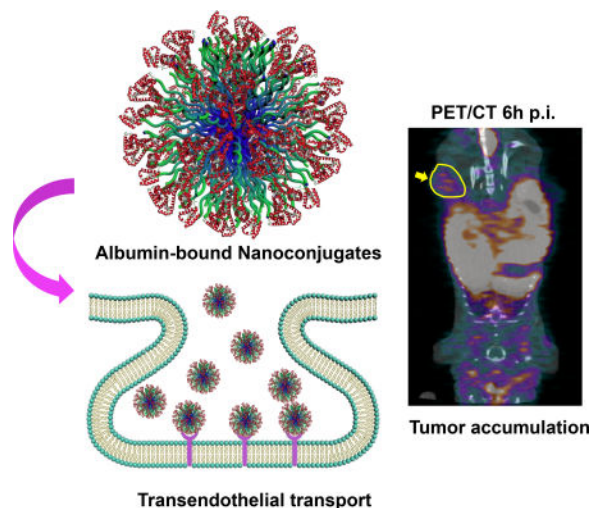
Keywords

Nanoconjugate drug delivery; Albumin-functionalized nanoparticles; Caveolae-mediated transcytosis; Cancer targeting; MCF-7 breast cancer

Polymeric-drug conjugated nanoparticles, often called nanoconjugates (NCs), have been extensively developed and exploited as promising drug carriers to deliver therapeutics to tumors, but their clinical applicability has yet to be demonstrated.[1–2] A major challenge to the development of NCs is the difficulty of delivering them to tumors efficiently. The current widely accepted passive cancer targeting mechanism of NCs is enhanced permeability and retention (EPR) effect, which refers to the preferential accumulation of NCs in tumors facilitated by the highly permeable nature of the tumor vasculature and poor lymphatic drainage of the interstitial fluid surrounding a tumor.[3] Many NC platforms are developed to fulfill the requirements of passive targeting by improving their pharmacokinetic profile in order to achieve time-dependent accumulation in tumor tissues. However, the targeting efficiency based on this mechanism is largely dependent on the leakiness of tumor blood vessels while heterogeneous distribution of pore sizes in tumor endothelial junctions has been observed both between (inter-tumor heterogeneity)[44] and within tumors (intra-tumor heterogeneity).[5] Such heterogeneity largely impairs effective extravasation of NCs from tumor vascular-endothelial barrier into tumor tissues via EPR effect.[4–5] As such, NCs need a portal to bypass the tumor endothelium barrier and effectively deliver therapeutics to cancer cells.

The caveolae are flask-shaped membrane invaginations of 50–100 nm in diameter, occupying as much as 70% of the endothelial membrane in blood capillaries, and play a major role in transporting macromolecules (size > 3nm) across the endothelial barrier.[6–7] Albumin, the most abundant protein in the blood, is able to transport across the endothelium membrane through caveolae-mediated transcytosis pathway.[8] The whole process starts with albumin binding to its receptor, a 60-kDa glycoprotein (gp60) on endothelial luminal surface

to initiate gp60 clustering and subsequent interacting with caveolin-1, the primary structural protein of caveolae.[9–10] The downstream signaling pathway is triggered to release caveolae from plasma membrane and induce transcellular transport of receptor-bound and fluid phase albumin.[11–12] Due to its inherent biocompatibility and lack of immunogenicity, albumin has been widely employed as drug carriers to deliver small-molecule chemotherapeutic agents for cancer treatment.[13–18] One of the examples is Abraxane, albumin-bound paclitaxel, which has been approved by US Food and Drug Administration (FDA) for the treatment of a wide variety of cancer types.[15, 19] In addition to binding with small-molecule chemotherapeutic drugs, albumin is also utilized as surface modification of nanoparticles to increase the water solubility, biocompatibility and to achieve long blood circulation time.[20–24] Nonetheless, taking advantage of biological function of albumin to facilitate NCs to transpass tumor endothelial barrier has been rarely explored.[25]

Here, we describe a broadly applicable strategy to improve cancer targeting efficiency of NCs by exploiting albumin's role as a "Trojan Horse" to facilitate the transport of NCs across tumor endothelium barrier and subsequently enhance their accumulation in the tumor tissues. By incorporating the aromatic albumin-binding domains into the polymer backbones, we designed an albumin-bound, Doxorubicin (Doxo) containing poly(phenyl *O*-carboxyanhydride) nanoconjugate, termed as Alb-NC, for targeting MCF-7 human breast cancer xenograft in athymic nude mice. MCF-7 has been reported to have limited vascular permeability among a variety of breast cancer cell lines, being hardly accessible by NCs relying on EPR effect, and therefore serve as an ideal preclinical model for assessing the tumor targeting capability of Alb-NCs. We report for the first time that Alb-NCs are highly effective for transporting across the tumor vascular endothelium and delivering chemotherapeutic reagents to tumor tissues through caveolae-mediated pathway, resulting in markedly improved anticancer activities compared to conventional PEGylated NCs (PEG-NCs). In addition, the Alb-NCs are easily formulated with well-controlled physicochemical properties, including high drug loading, quantitative drug loading efficiency, and controlled particle size with narrow particle size distribution in large scale. As such, the development of Alb-NCs has the potential to improve the therapeutic effectiveness of targeted cancer therapy for diverse solid tumors, and provides a simple, low-cost, controllable and scalable formulation to improve the cancer targeting efficiency and therapeutic effectiveness of nanomedicine.

RESULTS

Controlled formulation of Doxo-PheLA NCs comprising aromatic albumin-binding domains

Previous studies have suggested the albumin binding capability of a compound significantly increases as the number of aromatic rings in the compound increases.[26] The reason is presumably due to the Sudlow's site II domain in human serum albumin that has a high affinity for lipophilic and particularly aromatic compounds.[26–27] Thus, we aim to design a polymeric NC platform containing aromatic albumin-binding domains to achieve optimal albumin binding capacities (Scheme 1). We first chose phenylalanine to synthesize phenyl *O*-carboxyanhydrides (Phe-OCA),[28] the monomer bearing aromatic functionalities. Followed by the similar strategy as we previously developed,[28–30] Doxo was used as a

hydroxyl-containing drug to initiate the polymerization of Phe-OCA with the aid of a site- and chemo-selective metal catalyst, *i.e.*, (BDI-EI)ZnN(TMS)$_2$ to prepare Doxo-poly(Phe-OCA) conjugates, termed Doxo-PheLA (Scheme 1). This method is capable of producing a large scale of Doxo-PheLA conjugates with predetermined and tunable drug loading, and nearly 100% drug incorporation efficiency. The prepared Doxo-PheLA polymer conjugate with twenty-five repeating units had drug loading of Doxo as high as 10.3 *wt*%. The obtained Doxo-PheLA polymer was then nanoprecipitated into water to form Doxo-PheLA nanoconjugates (Doxo-PheLA NCs) (Scheme 1). The resulting NCs are 75 nm in diameter with relatively narrow particle size distribution (polydispersity = 0.070) as measured by DLS (Figure S1).

Albumin binding capability of Doxo-PheLA NCs

The aromatic functional groups on the side chains of Doxo-PheLA polymer were expected to render the resulting NCs with high binding affinity with albumin. We first used fluorescence correlation spectroscopy (FCS),[31] a technique which can quantitatively *in situ* to assess the radius of Alb-NCs by measuring the bursts of fluorescence emitted from NCs diffusing through a tiny spot volume formed by a tight focusing of excitation beam. Based on the fact that the concentration of albumin ranges from 400 to 675 μM in human blood,[8] we prepared a series of concentrations of albumin solution ranging from 1 μM to 1000 μM for the study. As Figure 1A showed, the hydrodynamic radius of Alb-NCs increased from 54 to 156 nm as the concentration of albumin increased from 1–1000 μM, indicating the albumin adsorption on the surfaces of NCs (Figure 1A, Table S1). To determine whether the binding between Doxo-PheLA NCs and albumin was attributed to the aromatic structures on the polymer side chains, we formulated Doxo-polylactide nanoconjugates (Doxo-PLA NCs)[32–34] with methyl side chains and studied their binding capability with albumin as compared to those of Doxo-PheLA NCs. We dispersed both Doxo-PheLA NCs and Doxo-PLA NCs into FITC-labeled albumin solution and further incubated them for 1 h at rt. When Doxo-PheLA NCs were pelleted and removed, the fluorescence intensity of the supernatant was significantly dropped by 80% (Figure 1B), owing to the large percentage of FITC-albumin bound to PheLA NCs and removed from the solution, while the fluorescence intensity of FITC-albumin incubated with Doxo-PLA NCs only decreased by 15% (Figure 1B), indicating significantly lower binding affinity between albumin and PLA NCs. The results clearly demonstrated the aromatic ring structure of the polymer chain contributed to the strong binding affinity of Doxo-PheLA NCs to albumin.

To further study whether the binding between albumin and Doxo-PheLA NCs are stable in the physiological condition, we dispersed Alb-NCs into human serum and incubated for 30 min, then collected the NCs by ultracentrifugation after several extensive wash. SDS–polyacrylamide gel electrophoresis (SDS–PAGE) analysis showed the exactly same albumin band between 48 and 74 kDa of Alb-NCs recovered from human serum (right column) as compared to pure Alb-NCs (left column), demonstrating the stable binding of albumin on the surfaces of Doxo-PheLA NCs in serum (Figure 1C). In addition, the binding between albumin and Doxo-PheLA NCs was demonstrated to be stable during cellular internalization process, as evidenced by the co-localization of NCs (red) and FITC-albumin (green) in the

MCF-7 human breast cancer cells under confocal laser scanning microscopy (CLSM) (Figure 1D).

Caveolae-mediated transcytosis of Alb-NCs across endothelial cell barrier

Prior studies have reported that the caveolae-mediated transcytosis is the primary mechanism of albumin transendotherlial permeability.[10] The binding of albumin to the albumin-binding protein (ABP) such as gp60 localized in caveolae played an essential role in mediating the transcellular transport of albumin across endothelial cell barriers.[9] Thus, we hypothesized Alb-NCs could exploit the biological functions of albumin displaying on the surfaces to efficiently overcome tumor endothelial barriers via caveolae-mediated transcellular transport mechanism (Figure 2A). To test this hypothesis, we carried out a time-course study to investigate the transendothelial transport process of Alb-NCs. Human Umbilical Vein Endothelial Cells (HUVEC) were grown to confluence on transwell membrane inserts to mimic the endothelial barrier. Alb-NCs in the Opti-MEM medium were incubated in the upper transwells above the HUVECs layer. At different time points, the fluorescence intensities of aliquots from the bottom plate wells were measured and converted to the concentrations of Alb-NCs in the medium using a predetermined calibration curve between the fluorescence intensity and the Alb-NCs concentration. As shown in Figure 2B, Alb-NCs demonstrated the rapid and efficient transendothelial transport with 44.4% Alb-NCs across the HUVECs barrier within 24 h. As a comparison, we formulated PEG-NCs with similar size as Alb-NCs and studied their capabilities across the HUVECs barrier. The result showed the transendothelial transport of PEG-NCs was only 18.2% in 24 h, two fold less than that of Alb-NCs (Figure 2B). The Alb-NCs significantly outperformed PEG-NCs, which could potentially improve the targeting efficiency and substantially enhance the therapeutic efficacy in some tumor types with less leaky tumor vasculature and limited EPR effects.

To further address the role of caveolae in transporting of Alb-NCs across endothelial barriers, both Alb-NCs and PEG-NCs were incubated with HUVECs for 4 h at 37°C in the presence of FITC labelled cholera toxin B (FITC-CTB, green), a marker for caveolae-specific ganglioside GM1.[35] CLSM images clearly showed the differences between Alb-NCs and PEG-NCs with respect to the cellular internalization processes. The internalized Alb-NC (red fluorescence) notably co-localized with CTB (green fluorescence), suggesting the caveolae is responsible for the uptake and transport of Alb-NCs in HUVECs (Figure 2C), while the red and green fluorescence were largely separated in HUVECs incubated with PEG-NCs, thus clearly indicating that the uptake of PEG-NCs followed the different mechanism from caveolae-mediated internalization (Figure 2C). Furthermore, we disturbed the organization of caveolae by treating HUVECs with methyl-β-cyclodextrin (CD) and measured the uptake of Alb-NC in endothelial cells. As shown in Figure 2D, methyl-β-CD largely prevented the internalization of Alb-NC in HUVECs. These results collectively support our hypothesis that Alb-NCs have the capability of transporting across the endothelial-cell barrier via caveolae-mediated transcytosis pathway. This effect may offer more benefits for the accumulation of Alb-NCs in the tumor tissues.

In vivo cancer targeting of Alb-NCs in MCF-7 human breast cancer xenograft

The enhanced transendothelial transport of Alb-NCs compared to PEG-NCs suggests that surface functionalization of NCs with albumin may potentially improve their *in vivo* cancer targeting. To explore this, Alb-NCs and PEG-NCs were radio-labelled with positron emitting isotope ^{64}Cu (denoted as ^{64}Cu-Alb-NC and ^{64}Cu-PEG-NC respectively), and then administered into athymic nude mice bearing subcutaneous (s.c.) MCF-7 human breast cancer xenograft. MCF-7 is an estrogendependent, noninvasive human breast cancer model that has been extensively studied and demonstrated to be with least vascular permeability among a variety of human breast cancer xenografts including MDA-MB-435, MDA-MB-231 and ZR75.[36–37] The NCs biodistribution were closely monitored by non-invasive whole body micro-positron emission tomography/X-ray computed tomography (micro-PET/CT) images after intravenous injection. Figure 3A demonstrated the noticeable radioactivity accumulation in the MCF-7 tumor of a representative mice injected with ^{64}Cu-Alb-NCs (yellow arrow, 0.5 % injected dose per gram of tissue (% I.D.g^{-1})) as early as 1 h post injection (p.i.). The signal was detected to be gradually increasing to 1.3 % I.D.g^{-1} 6 h p.i. and maintained as long as 24 h (1.4 % I.D.g^{-1}). Whereas in comparison, the signal detected in the tumor of mice treated with ^{64}Cu-PEG-NCs was 44.4% less (0.9 versus 1.3 % I.D.g^{-1}) 6 h p.i and 133.3% less (0.6 versus 1.4 % I.D.g^{-1}) 24 h p.i.. The area under curve (AUC) of ^{64}Cu-Alb-NCs was 1.55 times greater than that of ^{64}Cu-PEG-NCs during 24-h period, suggesting that the ^{64}Cu-Alb-NCs maintained overall higher concentration in the MCF-7 tumors. This sharp contrast was further confirmed by *ex vivo* measurement of the radioactivity in the excised tumors 24 h p. i. with the γ-counter. The result demonstrated that the accumulation of ^{64}Cu-Alb-NCs markedly increased in MCF-7 tumors (1.7 % I.D. g^{-1}) compared to that of ^{64}Cu-PEG-NCs (0.98 % I.D. g^{-1}) (Figure S3A). The accumulation of ^{64}Cu-Alb-NCs and ^{64}Cu-PEG-NCs in the blood and other organs were also assessed by γ-counter (Figure S3B). The results showed ^{64}Cu-Alb-NCs accumulated to a less extent within reticuloendothelial organs than ^{64}Cu-PEG-NCs, whereas a higher accumulation of ^{64}Cu-Alb-NCs than ^{64}Cu-PEG-NCs were noticed in heart and lung, which was presumably due to the high caveolin-1 expression in these two microvessel-rich organs.[6]

To further evaluate the tissue distribution of accumulated Alb-NCs in the MCF-7 tumors, Alb-NCs and PEG-NCs were administered into the mice bearing MCF-7 xenografts through intravenous (i.v.) injection, respectively. The tumors were dissected 6 h p.i., stained, and analyzed with CLSM. Substantially increased red signals from Doxo were observed along the tumor blood vessels (green, stained with CD31) of mice injected with Alb-NCs, indicating that more Alb-NCs had passed through blood vessels into adjacent tumor tissue than PEG-NCs. Further quantification with Image J further confirmed 1.8-fold increase in tumor accumulation of Alb-NCs compared with PEG-NCs (Figure 3D). Collectively, these results supported that Alb-NCs exerted greater accumulation in poorly permeabilized MCF-7 breast cancer model than PEG-NCs, presumably as a consequence of their enhanced transendothelial transport capability.

Efficacy of Alb-NCs against MCF-7 human breast cancer xenograft

Given the preferential tumor accumulation of Alb-NCs in MCF-7 model demonstrated by micro-PET/CT images and CLSM images, we hypothesized that improved antitumor

efficacy could be achieved by Alb-NCs. To determine their therapeutic potential, we used s.c. implanted MCF-7 human breast cancer xenografts as a model for evaluation. Mice bearing MCF-7 tumors were randomly divided into three groups to minimize the differences with respect to tumor size and body weight among groups at Day 0. Two groups of mice received the intravenous injection of Alb-NCs and PEG-NCs at the dose of 40 mg Doxo per kg mice body weight (40 mg/kg) every four days for three times, respectively. Another group of mice received PBS as a negative control (Figure 4A). The tumor sizes in each group were monitored up to 56 days post injection. Compared with the PBS negative control group, mice treated with Alb-NCs showed significantly delayed tumor growth ($p < 0.001$, two-tailed T test with welch's correction) while there was no statistically significant difference between PEG-NCs treatment and PBS ($p = 0.064$) (Figure 4B). Treatment of Alb-NCs resulted in markedly smaller average tumor size (568 ± 87 mm^3) at day 56 in comparison with PEG-NCs (961 ± 62 mm^3) and PBS (1533 ± 198 mm^3) (Figure 4B and Figure S4), demonstrating that Alb-NCs is much more effective than PEG-NCs in delaying tumor growth. Importantly, the survival rate of mice treated with Alb-NCs was also markedly higher than mice treated with PEG-NCs and untreated mice (Figure 4C). All together, these results provide definitive evidence supporting that Alb-NCs exhibited far superior efficacy against MCF-7 human breast cancer xenografts than PEG-NCs in athymic nude mice in terms of inhibiting tumor growth and elongating the mice survival. At the meantime, no significant body weight drop (Figure S5) or abnormal behaviors among all of groups were observed, indicating no obvious toxicities observed for Alb-NCs.

DISCUSSION

In the past several decades, EPR effect has been considered as a landmark principle in designing the nanoparticle (NP)-based drug delivery systems for cancer therapy. PEGylation has been the routine NP surface modification method to avoid complement protein mediated opsonization and to elongate the circulation of NPs in order to take advantage of the EPR effect.[38–39] However, the broad heterogeneity of tumor vasculatures observed among different tumor types and/or within individual tumors often complicates the delivery of PEGylated NPs. The stealth effect of PEG is reported to largely reduce the interaction of NPs and living organism, impeding the effective penetration of NPs across the vascular endothelium barrier, and leading to low accumulation in the tumor tissues.[40] Moreover, recent studies suggested that PEGylation may lead to accelerated blood clearance of NPs upon repeated injections due to the production of PEG-specific IgM and subsequent activation of the complement system.[41] These factors collectively may lead to diminished effectiveness of PEGylated therapeutics As the most abundant protein in the human blood, albumin exhibits great biocompatibility, less toxicity, lack of immunogenicity and easy accessibility, showing great promise in the surface functionalization of NCs as PEG alternatives. In this investigation, Alb-NCs, easily attainable with controlled size (sub-100 nm), narrow particle size distribution, pre-determined, high Doxo loading and ~100% loading efficiency, markedly outperformed the control PEG-NCs in biodistribution and accumulation in the transnationally relevant, poorly permeable MCF-7 human breast cancer model *in vivo*. Such increased *in vivo* cancer targeting activity is attributed to the enhanced transendothelial transport of Alb-NCs facilitated by albumin, which subsequently lead to

greatly enhanced antitumor efficacy compared to PEG-NCs in MCF-7 model. A myriad of examples have been reported that albumin are utilized as drug delivery vehicles to largely improve therapeutic efficacy. Our results unravel the transendothelial transport mechanism for albumin-functionalized polymeric NCs, and demonstrate such unique *in vivo* behaviors lead to potential benefits in cancer targeting and improvement in therapeutic efficacy across different cancer types particularly in tumors with limited EPR effect. To our knowledge, this is the first demonstration of using albumin as surface functionalization of NPs for transporting across tumor-endothelial barriers to improve their *in vivo* cancer targeting efficiencies. As no bioconjugation is needed for the coating of albumin to the NCs, this simple formulation process of Alb-NCs may allow for a large scale of production of NCs with well-controlled physicochemical properties, and hence potentially facilitates clinical translation.

CONCLUSIONS

In conclusion, we developed a polymeric NC platform comprised of Doxo-PheLA and surface functionalization of albumin for transportation across tumor endothelial barrier to facilitate *in vivo* cancer targeting. These NCs showed improved antitumor efficacy in poorly permeabilized human MCF-7 breast cancer xenograft model compared to conventional PEG-NCs. Our findings further demonstrated that the albumin played a critical role in facilitating cancer targeting of the formulated NCs via caveolae-mediated transcytosis pathway. The well-controlled physicochemical properties as well as favorable *in vivo* behaviors of the Alb-NCs demonstrate their great potential in drug delivery applications.

METHODS

Materials

Doxo·HCl was purchased from Bosche Scientific (New Brunswick, NJ, USA). D,L-Lactide (LA) was purchased from TCI America (Portland, OR, USA). (S)-2,2',2'',2'''-(2-(4-isothiocyanatobenzyl)-1,4,7,10-tetraazacyclododecane-1,4,7,10-tetrayl)tetraacetic acid (*p*-SCN-Bn-DOTA) was purchased from Macrocyclics, Inc. (Dallas, TX, USA). All the other chemicals were purchased from Sigma–Aldrich (St Louis, MO, USA). Anhydrous tetrahydrofuran (THF), dimethylformamide (DMF), and dichloromethane (DCM) were purified by alumina columns and kept anhydrous by using molecular sieves.

Instrumentation

The molecular weights (MWs) and molecular weight distribution (MWD) of PheLA were determined by gel permeation chromatography (GPC, also known as size exclusion chromatography (SEC)) equipped with an isocratic pump (Model 1100, Agilent Technology, Santa Clara, CA, USA), a DAWN HELEOS 18-angle laser light scattering detector and an Optilab rEX refractive index detector (Wyatt Technology, Santa Barbara, CA, USA). The wavelength of the HELEOS detector was set at 658 nm. The size exclusion columns (Phenogel columns 100, 500, 10^3 and 10^4 Å, 5 μm, 300 × 7.8 mm, Phenomenex, Torrance, CA, USA) used for the analysis of polymer-drug conjugates was serially connected on the GPC. The GPC columns were eluted with DMF (HPLC grade) containing 0.1 M LiBr at

65 °C at 1 mL/min. Data processing was performed with ASTRA V software (Version 5.1.7.3, Wyatt Technology, Santa Barbara, CA, USA). HPLC analyses were performed on a System Gold system equipped with a 126P solvent module and a System Gold 128 UV detector (Beckman Coulter, Fullerton, CA, USA) equipped with a 126P solvent module, a System Gold 128 UV detector and an analytical C18 column (Luna C18, 250 × 4.6 mm, 5 μ, Phenomenex, Torrance, CA, USA). Infrared spectra were recorded on a PerkinElmer 100 serial FT-IR spectrophotometer (PerkinElmer, Waltham, MA, USA). The sizes and the size distributions of the nanoconjugates (NCs) were determined on a ZetaPALS dynamic light scattering (DLS) detector (15 mW laser, incident beam = 676 nm, Brookhaven Instruments, Holtsville, NY, USA). *Ex vivo* measurement of the radioactivity was conducted with 2480 Wizard2 Automatic γ-counter (Perkin-Elmer, USA). The flash frozen organs were embedded with optimum cutting temperature (O.C.T.) compound (Sakura Finetek USA, Torrance, CA, USA) and sectioned with a Leica CM3050S cryostat and mounted on glass slides for histological analysis.

Cell lines

MCF-7 cells were obtained from ATCC (Manassas, VA, USA). Cells were cultured in DMEM medium containing 10% fetal bovine serum (FBS), 100 units/mL aqueous Penicillin G and 1 nM estrogen (Sigma-Aldrich Inc., St. Louis, MO, USA). Human umbilical vein endothelial cells (HUVEC) were purchased from ATCC (Manassas, VA, USA) and cultured in Human Endothelial Cell Media from Cell Applications, Inc. (San Diego, CA, USA). Both of the cells were grown at 37 °C in 5% CO_2 humidified air. The confocal microscopy images for cellular internalization studies were taken on a Zeiss LSM700 Confocal Microscope (Carl Zeiss, Thornwood, NY, USA) using a 63×/1.4 oil lens.

Animals

Female athymic nude mice (5–6 weeks old) were purchased from the National Cancer Institute (NCI, Frederick, MD, USA) and ovariectomized at the age of 21 days by the vendor. After arrival, mice were single-cage housed and had free access to food and water. Food and water were available *ad libitum*. Artificial light was provided in a 12/12 hour cycle. All animal procedures were performed in accordance with the Guidelines for Care and Use of Laboratory Animals of Illinois Institutional Animal Care and Use Committee (IACUC) and approved by the Animal Ethics Committee of University of Illinois.

Preparation and characterization of Doxo-PheLA$_{25}$ conjugate

In a glovebox, Doxo (12.5 mg, 0.02 mmol) was dissolved in anhydrous tetrahydrofuran (THF, 600 μL) and mixed with a 900 μL THF solution containing (BDI-EI)ZnN(TMS)$_2$ (13.0 mg, 0.02 mmol). The mixture was stirred for 15 min. Phe-OCA (96.0 mg, 25 equiv.) was dissolved in THF (2 mL) and added to above solution under stirring. The reaction proceeded in the glovebox overnight. The conversion of Phe-OCA was determined by FT-IR (by monitoring the disappearance of anhydride band at 1812 cm^{-1}). After Phe-OCA was completely consumed, the reaction was stopped by quenched with cold methanol solution (300 μL). Then, the polymer was precipitated with ether (50 mL) and dried by vacuum. The Doxo incorporation efficiency was determined by HPLC. No free Doxo peek was identified after polymerization indicating nearly 100% drug incorporation efficiency.

Synthesis of 1,4,7,10-tetraazacyclododecane-1,4,7,10-tetraacetic acid (DOTA)-PheLA$_{25}$ conjugate

The NH$_2$-PheLA$_{25}$ conjugate was synthesized by following a similar procedure as previously published by using ethanolamine as the initiator[28]. In a reaction vial containing NH$_2$-PheLA$_{25}$ conjugates (23.5 mg, 0.004 mmol) was added an anhydrous dimethylformamide (DMF) solution (0.5 mL) of DOTA-NCS (2.2 mg, 0.018 mmol) and triethylamine (3.6 mg, 0.036 mmol). The reaction mixture was stirred for 4 h under nitrogen at rt. The solvent and triethylamine were removed under vacuum to give DOTA-PheLA$_{25}$, which was used directly without further purification.

General procedure for the preparation and characterization of Doxo-PheLA$_n$ nanoconjugates (NCs)

A DMF solution of the Doxo-PheLA$_{25}$ conjugate (100 μL, 10 mg/mL) was added dropwise to nanopure water (2 mL). The resulting Doxo-PheLA$_{25}$ NCs were collected by ultrafiltration (5 min, 3000 × g, Ultracel membrane with 100,000 NMWL, Millipore, Billerica, MA, USA), washed with water and then characterized by DLS for particle sizes and size distributions.

Preparation and characterization of albumin-functionalized Doxo-PheLA$_{25}$ nanoconjugates (Alb-NCs)

The obtained Doxo-PheLA$_{25}$ NCs were dispersed in nanopure water (2 mL, 0.5 mg/mL). Human serum albumin (HSA) (5 mg) was added into the NC solution and stirred for 30 min at rt. The resulting HSA-bound Doxo-PheLA$_{25}$ NCs (Alb-NCs) were collected and washed with nanopure water by ultrafiltration (5 min, 3000 × g, Ultracel membrane with 100,000 NMWL, Millipore, Billerica, MA, USA), and then characterized by DLS for particle sizes and size distributions.

Preparation and characterization of PEGylated Doxo-PheLA$_{25}$ nanoconjugates (PEG-NCs)

A diblock polymer of mPEG$_{5k}$-PheLA$_{100}$ was synthesized by following the procedures as previously published by using mPEG$_{5k}$-OH as the initiator.[28] A DMF solution of the mixture of Doxo-PheLA$_{25}$ conjugate (50 μL, 20 mg/mL) and mPEG$_{5k}$-PheLA$_{100}$ (50 μL, 20 mg/mL) was added dropwise to nanopure water (2 mL). The resulting PEGylated Doxo-PheLA$_{25}$ (PEG-NCs) were collected by ultrafiltration (5 min, 3000 × g, Ultracel membrane with 100,000 NMWL, Millipore, Billerica, MA, USA), washed with water and then characterized by DLS for particle sizes and size distributions.

DLS measurements

The hydrodynamic size was measured with 90Plus Particle Size Analyser by dispersing the NPs in DI water at concentration of 0.5 mg/mL. Measurements were taken at a 90° scattering angle.

Preparation of ^{64}Cu labeled Alb-NCs or PEG-NCs

The ^{64}Cu chloride (300 μCi, obtained from Washington University at St. Louis, MO, USA) was mixed with Alb-NCs or PEG-NCs (20 mg) in NH$_4$OAc buffer (pH = 5.5, 0.1 M, 0.5

mL). The mixture was incubated for 1 h at 60 °C. To determine the labeling efficiency and labeling stability, the NCs were washed by ultrafiltration (10 min, 3000 × g, Ultracel membrane with 100,000 NMWL, Millipore, Billerica, MA, USA), and the radioactivity in the supernatant and the NC solution was measured at different time points respectively. The ^{64}Cu labeling efficiency in ^{64}Cu-Alb-NCs and ^{64}Cu-PEG-NCs were 90.27% and 84.87%, respectively. The labeling stability was shown in Figure S2. The purified ^{64}Cu-labelled NCs were used for injection.

Fluorescence Correlation Spectroscopy measurements

FCS measurements were made on a home-built instrument using an 800 nm pulsed light source (Spectra Physics Mai Tai) for two-photon excitation. The excitation beam was focused to a spot size of roughly 400 nm, and the fluorescence of Alb-NCs diffusing through the focal volume was detected on a single-photon counter (ID Quantique). The resulting time trace reveals bursts of fluorescence, the auto-correlation of which can be related to the diffusion constant of the labeled particles. The diffusion constant is extracted by fitting the experimental data with Eq 1.

$$G(\tau) = G(0)\frac{1}{\left(1 + \frac{\tau}{\tau_D}\right)\left(1 + \frac{\omega_Z}{\omega_{xy}}^{-2}\left(\frac{\tau}{\tau_D}\right)\right)^{1/2}} \quad (1)$$

Here, ω accounts for the focal spot dimensions, and τ_D is the relaxation time of the autocorrelation curve. From the relaxation time, the diffusion constant can be determined by:

$$D = \frac{\omega_{xy}^2}{4\tau_D} \quad (2)$$

Finally, the measured diffusion constant can be directly related to the radius of the diffusing particle through the Stokes-Einstein equation.

$$D = \frac{k_B T}{6\pi\eta_s R} \quad (3)$$

FCS measurements were made of the Alb-NCs as a function of serum albumin concentration, and the resulting nanoparticle radius was determined for each concentration (Table S1).

Albumin binding measurements

Doxo-PheLA NC solution (2 mL, 0.5mg/mL) or Doxo-PLA NC solution (2 mL, 0.5mg/mL) prepared as previously reported was added into FITC labeled human serum albumin (FITC-albumin) solution (2 mL, 0.5mg/mL) and further incubated for 1 h at rt. Then NCs were pelleted and removed. The fluorescence intensity of supernatant of FITC-albumin was

measured by fluorescence spectrometer to determine the amount of FITC-albumin left in the solution. The FITC-albumin solution without any NC was used as a control to calculate the loss of albumin during centrifugation process.

SDS-PAGE study

Alb-NCs (1 mL, 10mg/mL) were dispersed in either PBS (1 mL) or 50% human serum (1 mL, human serum/PBS= 1:1) and incubated at 37 °C for 30 min. Then NCs were washed and collected by ultrafiltration (5 min, $3000 \times g$, Ultracel membrane with 100,000 NMWL, Millipore, Billerica, MA, USA) and then analyzed by SDS-PAGE.

Cellular internalization of Alb-NCs in MCF-7 breast cancer cells

The Alb-NCs were prepared by incubation of Doxo-PheLA NCs with FITC-Albumin as described before. The MCF-7 cells were grown in chamber slides at concentrations to allow 70% confluence in 24 h. On the day of experiments, the medium was removed and washed with PBS (500 μL), and then incubated with pre-warmed opti-MEM medium for 30 min before the addition of the Alb-NCs (1 mg/mL). The cells were co-incubated with Alb-NCs for 2 h at 37 °C and then washed with PBS (500 μL) twice, fixed with 4% formaldehyde. The cell nucleus was stained with 4',6-diamidino-2-phenylindole (DAPI) and imaged by confocal laser scanning microscopy (CLSM).

Cellular internalization of Alb-NCs in HUVECs

The HUVECs were grown in chamber slides at concentrations to allow 70% confluence in 24 h. On the day of experiments, the medium was removed and washed with PBS (500 μL), and then incubated with pre-warmed opti-MEM medium for 30 min before the addition of the Alb-NCs (1 mg/mL) or PEG-NCs (1 mg/mL). For co-localization study, HUVEC cells were co-incubated with Alb-NCs or PEG-NCs in the presence of FITC labeled cholera toxin B (FITC-CTB) for 4 h at 37 °C. The cells were then washed with PBS (500 μL) twice, fixed with 4% formaldehyde and subsequently imaged by confocal laser scanning microscopy (CLSM). For inhibition study, HUVEC cells were incubated with methyl-β-cyclodextrin (5 mM) in PBS for 20 min at 37 °C before the addition of Alb-NCs. Then HUVECs were incubated with Alb-NCs (1 mg/mL) for 4 h at 37 °C. The nucleus was stained with DAPI (blue) and the cell skeleton was stained with Alexa Fluor® 488 Phalloidin (green) and imaged by confocal laser scanning microscopy (CLSM).

Transcytosis study

HUVECs were grown to confluence forming the monolayer using Costar transwell units (0.4-μm pore sizes, 6.5 mm diameter for 24 well plate).[42]. The HUVEC monolayers were washed and incubated in opti-MEM 30 min prior to experiments. The upper transwells were filled with 0.1 mL of Alb-NCs or PEG-NCs (5 mg/mL) and the lower culture plate wells filled with 1 mL opti-MEM. At scheduled time points (1 h, 2 h, 4 h, 6 h, and 24 h), 50 μL samples from the lower compartment were collected and diluted ($100 \times$) for measuring the fluorescence intensity of Doxo by fluorescence spectrometer. The amount of NCs across HUVEC monolayer was calculated using calibration curve. 50 μL opti-MEM was added after each sample collection to keep the volume in the lower culture plate wells constant.

Micro-PET/CT imaging evaluation

Six female athymic nude mice were prepared for the implantation of MCF-7 breast cancer cells. MCF-7 cells (1×10^6) were suspended in a 1:1 mixture of Hank's Balanced Salt (HBS) buffer and matrigel, and then injected subcutaneously into the flank of a mouse. When tumors reached ~100 mm^3, mice were divided into 2 groups (n=3), minimizing weight and tumor size difference among the groups. The two groups of mice were treated with ^{64}Cu-Alb-NCs or ^{64}Cu-PEG-NCs at a dose of 40 μCi and 43 μCi intravenously, respectively. Mice were placed on the micro-CT imaging bed and kept anaesthetized with a constant isoflurane flow. A dynamic PET scan was acquired for 1 h (60 min acquisition time, reconstructed as 60 frames at 60 seconds/frame). The micro-CT scan (80 keV/500 μA X-rays energy, 360 projections, 360 degrees, 75 μm pixel size) was used for determining the anatomical localization of the tumor. Static micro-PET scans were acquired at two selected time points (6 h and 24 h p.i.) together with micro-CT scans for anatomical co-registration. The obtained micro-PET and micro-CT images were constructed using ordered subset expectation maximization and cone-beam algorithms with existing commercial software (Inveon Acquisition Workspace and Cobra Exxim, respectively). To quantify the radioactivity of ^{64}Cu in the tumors, complex irregular volumes of interest (VOIs) were drawn on the micro-CT images and registered with micro-PET images to determine mean counts in each VOI. The radiotracer activity from each VOI was normalized by injected dose and expressed at percent of the decay-corrected injected activity per cm^3 of tissue, which can be approximated as percentage % I.D. g^{-1} assuming the density of the tissue is around 1g/cm^3. The initial total injected activity was determined by dose calibrator before injection.

In vivo biodistribution evaluation with γ-counter

After Micro-PET/CT imaging acquisition, mice were euthanized 24 h p.i. The blood and major organs (liver, spleen, kidney, heart, lung, intestine, bladder and muscle), as well as MCF-7 tumor were collected, weighed and measured for radioactivity (^{64}Cu) with a γ-counter (Wizard2, Perkin-Elmer, USA) using appropriate energy window centered at photo peak of 511 keV. Raw counts were corrected for background, decay, and weight. Corrected counts were converted to microcurie per gram of tissue (μCi g^{-1}) with a previously determined calibration curve by counting the ^{64}Cu standards. The activity in blood and each collected tissue sample was calculated as percentage of the injected dose per gram of tissue (% I.D. g^{-1}). For this calculation, the tissue radioactivity was corrected for the ^{64}Cu decay (T(1/2)=12.7 h) to the time of γ-well counting.

In vivo tumor accumulation study

Athymic nude mice bearing MCF-7 tumors were injected intravenously with Alb-NCs and PEG-NCs (200μL, 20mg/kg Doxo equivalent) (n=3). The mice were sacrificed and the tumors were collected 6 h post injection. The tumor sections (5 μm in thickness) were collected by cryostat with a Leica CM3050S cryostat and mounted on glass slides. The nucleuses were stained by DAPI. The blood vessel was stained by anti-CD31 (FITC) antibody by incubating slides with primary CD31 antibody (1/100) at 4 °C overnight and then being stained with a FITC-conjugated secondary antibody (1/150) at 37 °C for 1 h in the dark. The stained tumor sections were analyzed by confocal fluorescence microscope

(Ziess, LSM700). Quantification of the accumulation of Alb-NCs and PEG-NCs in the tumor tissues by the averaging fluorescence intensity of Doxo per area (μm^2) by Image J.

In vivo efficacy study

Twelve female athymic nude mice were prepared for the implantation of MCF-7 breast cancer cells. MCF-7 cells (1×10^6) were suspended in a 1:1 mixture of Hank's Balanced Salt (HBS) buffer and matrigel, and then injected subcutaneously into the flanks of a mouse (four injection sites per mouse). When tumors reached ~110 mm^3, mice were divided into 3 groups (n=4), minimizing weight and tumor size difference among the groups. Tumor-bearing mice of the corresponding group were treated three times (every four days) through iv injection of PBS ($1\times$, 200 μL), PEG-NCs (40 mg Doxo/kg) and Alb-NCs (40 mg Doxo/kg), respectively. The body weight and tumor sizes of animals were monitored closely. The tumor size for each animal were monitored by using calipers without knowledge of which injection each animal had received. The tumor volume for each time point was calculated according to the formula (length) $\times$ (width)^2/2. If body weight loss is beyond 20% of predosing weight, the animals were euthanized. When the tumor load reached 900 mm^3 (as predetermined endpoint) or the animal had become moribund, the mouse was sacrificed. When an animal exited the study due to tumor size or treatment related death, the final tumor size recorded for the animal was included with the data used to calculate the mean size at subsequent time point. Curves were truncated after two or more deaths occurred.

Statistical Analyses

For efficacy study, unpaired T-Test (two tailed) with Welch's correction was used for statistical analysis. The results were deemed significant at $*p < 0.05$, $** \ p < 0.01$, $*** \ p < 0.001$. For other studies, student T-Test (two tailed) was used for statistical analysis. The results were deemed significant at $*p < 0.05$, $** \ p < 0.01$, $*** \ p < 0.001$.

Supplementary Material

Refer to Web version on PubMed Central for supplementary material.

Acknowledgments

References

1. Davis ME, Chen Z, Shin DM. Nanoparticle therapeutics: an emerging treatment modality for cancer. Nat Rev Drug Discov. 2008; 7(9):771–782. [PubMed: 18758474]

2. Egusquiaguirre SP, Igartua M, Hernandez RM, Pedraz JL. Nanoparticle delivery systems for cancer therapy: advances in clinical and preclinical research. Clin Transl Oncol. 2012; 14(2):83–93. [PubMed: 22301396]

3. Fang J, Nakamura H, Maeda H. The EPR effect: Unique features of tumor blood vessels for drug delivery, factors involved, and limitations and augmentation of the effect. Adv Drug Deliver Rev. 2011; 63(3):136–151.

4. Prabhakar U, Maeda H, Jain RK, Sevick-Muraca EM, Zamboni W, Farokhzad OC, Barry ST, Gabizon A, Grodzinski P, Blakey DC. Challenges and Key Considerations of the Enhanced Permeability and Retention Effect for Nanomedicine Drug Delivery in Oncology. Cancer Res. 2013; 73(8):2412–2417. [PubMed: 23423979]

5. Maeda H. Toward a full understanding of the EPR effect in primary and metastatic tumors as well as issues related to its heterogeneity. Adv Drug Deliver Rev. 2015; 91:3–6.

6. Sowa G. Caveolae, caveolins, cavins, and endothelial cell function: new insights. Front Physiol. 2012; 2

7. Wang Z, Tiruppathi C, Cho J, Minshall RD, Malik AB. Delivery of nanoparticle: complexed drugs across the vascular endothelial barrier via caveolae. IUBMB Life. 2011; 63(8):659–67. [PubMed: 21766412]

8. Tiruppathi C, Naqvi T, Wu YB, Vogel SM, Minshall RD, Malik AB. Albumin mediates the transcytosis of myeloperoxidase by means of caveolae in endothelial cells. P Natl Acad Sci USA. 2004; 101(20):7699–7704.

9. Minshall RD, Tiruppathi C, Vogel SM, Niles WD, Gilchrist A, Hamm HE, Malik AB. Endothelial cell-surface gp60 activates vesicle formation and trafficking via G(i)-coupled Src kinase signaling pathway. J Cell Biol. 2000; 150(5):1057–1069. [PubMed: 10973995]

10. Tiruppathi C, Song W, Bergenfeldt M, Sass P, Malik AB. Gp60 activation mediates albumin transcytosis in endothelial cells by tyrosine kinase-dependent pathway. J Biol Chem. 1997; 272(41):25968–25975. [PubMed: 9325331]

11. Shajahan AN, Timblin BK, Sandoval R, Tiruppathi C, Malik AB, Minshall RD. Role of Src-induced dynamin-2 phosphorylation in caveolae-mediated endocytosis in endothelial cells. J Biol Chem. 2004; 279(19):20392–400. [PubMed: 15007081]

12. Shajahan AN, Tiruppathi C, Smrcka AV, Malik AB, Minshall RD. Gbetagamma activation of Src induces caveolae-mediated endocytosis in endothelial cells. J Biol Chem. 2004; 279(46):48055–62. [PubMed: 15345719]

13. Elzoghby AO, Samy WM, Elgindy NA. Albumin-based nanoparticles as potential controlled release drug delivery systems. J Control Release. 2012; 157(2):168–182. [PubMed: 21839127]

14. Holding JD, Lindup WE, Vanlaer C, Vreeburg GCM, Schilling V, Wilson JA, Stell PM. Phase-I Trial of a Cisplatin-Albumin Complex for the Treatment of Cancer of the Head and Neck. Brit J Clin Pharmaco. 1992; 33(1):75–81.

15. Arpino G, De Placido S, De Angelis C. Nab-paclitaxel for the management of triple-negative metastatic breast cancer: a case study. Anti-Cancer Drug. 2015; 26(1):117–122.

16. Zhao D, Zhang H, Tao W, Wei W, Sun J, He Z. A rapid albumin-binding 5-fluorouracil prodrug with a prolonged circulation time and enhanced antitumor activity. Biomater Sci. 2017; 5(3):502–510. [PubMed: 28116362]

17. Zheng YR, Suntharalingam K, Johnstone TC, Yoo H, Lin W, Brooks JG, Lippard SJ. Pt(IV) prodrugs designed to bind non-covalently to human serum albumin for drug delivery. J Am Chem Soc. 2014; 136(24):8790–8. [PubMed: 24902769]

18. Arabi SH, Aghelnejad B, Schwieger C, Meister A, Kerth A, Hinderberger D. Serum albumin hydrogels in broad pH and temperature ranges: characterization of their self-assembled structures and nanoscopic and macroscopic properties. Biomater Sci. 2018

19. Gradishar WJ. Albumin-bound paclitaxel: a next-generation taxane. Expert Opin Pharmaco. 2006; 7(8):1041–1053.

20. Merlot AM, Kalinowski DS, Richardson DR. Unraveling the mysteries of serum albumin-more than just a serum protein. Front Physiol. 2014; 5

21. Chen Q, Liang C, Wang C, Liu Z. An Imagable and Photothermal "Abraxane-Like" Nanodrug for Combination Cancer Therapy to Treat Subcutaneous and Metastatic Breast Tumors. Adv Mater. 2015; 27(5):903–910. [PubMed: 25504416]

22. Chen Q, Liang C, Wang X, He JK, Li YG, Liu Z. An albumin-based theranostic nano-agent for dual-modal imaging guided photothermal therapy to inhibit lymphatic metastasis of cancer post surgery. Biomaterials. 2014; 35(34):9355–9362. [PubMed: 25132606]

23. Sheng ZH, Hu DH, Zheng MB, Zhao PF, Liu HL, Gao DY, Gong P, Gao GH, Zhang PF, Ma YF, Cai LT. Smart Human Serum Albumin-Indocyanine Green Nanoparticles Generated by Programmed Assembly for Dual-Modal Imaging-Guided Cancer Synergistic Phototherapy. Acs Nano. 2014; 8(12):12310–12322. [PubMed: 25454579]

24. Chakrabortty S, Sison M, Wu Y, Ladenburger A, Pramanik G, Biskupek J, Extermann J, Kaiser U, Lasser T, Weil T. NIR-emitting and photo-thermal active nanogold as mitochondria-specific probes. Biomater Sci. 2017; 5(5):966–971. [PubMed: 28282092]

25. Chen Q, Liu Z. Albumin Carriers for Cancer Theranostics: A Conventional Platform with New Promise. Adv Mater. 2016; 28(47):10557–10566. [PubMed: 27111654]

26. Ritchie TJ, Macdonald SJF. The impact of aromatic ring count on compound developability - are too many aromatic rings a liability in drug design? Drug Discov Today. 2009; 14(21–22):1011–1020. [PubMed: 19729075]

27. Zsila F, Bikadi Z, Malik D, Hari P, Pechan I, Berces A, Hazai E. Evaluation of drug-human serum albumin binding interactions with support vector machine aided online automated docking. Bioinformatics. 2011; 27(13):1806–1813. [PubMed: 21593135]

28. Yin Q, Tong R, Xu YX, Baek K, Dobrucki LW, Fan TM, Cheng JJ. Drug-Initiated Ring-Opening Polymerization of O-Carboxyanhydrides for the Preparation of Anticancer Drug-Poly(O-carboxyanhydride) Nanoconjugates. Biomacromolecules. 2013; 14(3):920–929. [PubMed: 23445497]

29. Yin Q, Yin LC, Wang H, Cheng JJ. Synthesis and Biomedical Applications of Functional Poly(alpha-hydroxy acids) via Ring-Opening Polymerization of O-Carboxyanhydrides. Accounts Chem Res. 2015; 48(7):1777–1787.

30. Wang H, Tang L, Tu CL, Song ZY, Yin Q, Yin LC, Zhang ZH, Cheng JJ. Redox-Responsive, Core-Cross-Linked Micelles Capable of On-Demand, Concurrent Drug Release and Structure Disassembly. Biomacromolecules. 2013; 14(10):3706–3712. [PubMed: 24003893]

31. Tian Y, Martinez MM, Pappas D. Fluorescence correlation spectroscopy: a review of biochemical and microfluidic applications. Appl Spectrosc. 2011; 65(4):115A–124A.

32. Yin Q, Tang L, Cai KM, Tong R, Sternberg R, Yang XJ, Dobrucki LW, Borst LB, Kamstock D, Song ZY, Helferich WG, Cheng JJ, Fan TM. Pamidronate functionalized nanoconjugates for targeted therapy of focal skeletal malignant osteolysis. P Natl Acad Sci USA. 2016; 113(32):E4601–E4609.

33. Tang L, Tong R, Coyle VJ, Yin Q, Pondenis H, Borst LB, Cheng JJ, Fan TM. Targeting Tumor Vasculature with Aptamer-Functionalized Doxorubicin - Polylactide Nanoconjugates for Enhanced Cancer Therapy. Acs Nano. 2015; 9(5):5072–5081. [PubMed: 25938427]

34. Tong R, Cheng JJ. Ring-Opening Polymerization-Mediated Controlled Formulation of Polylactide-Drug Nanoparticles. Journal of the American Chemical Society. 2009; 131(13):4744–4754. [PubMed: 19281160]

35. Blank N, Schiller M, Krienke S, Wabnitz G, Ho AD, Lorenz HM. Cholera toxin binds to lipid rafts but has a limited specificity for ganglioside GM1. Immunol Cell Biol. 2007; 85(5):378–382. [PubMed: 17325693]

36. Holliday DL, Speirs V. Choosing the right cell line for breast cancer research. Breast Cancer Res. 2011; 13(4):215. [PubMed: 21884641]

37. Bhujwalla ZM, Artemov D, Natarajan K, Ackerstaff E, Solaiyappan M. Vascular differences detected by MRI for metastatic versus nonmetastatic breast and prostate cancer xenografts. Neoplasia. 2001; 3(2):143–53. [PubMed: 11420750]

38. Jokerst JV, Lobovkina T, Zare RN, Gambhir SS. Nanoparticle PEGylation for imaging and therapy. Nanomedicine (Lond). 2011; 6(4):715–28. [PubMed: 21718180]

39. Cai KM, Wang AZ, Yin LC, Cheng JJ. Bio-nano interface: The impact of biological environment on nanomaterials and their delivery properties. J Control Release. 2017; 263:211–222. [PubMed: 28062299]

40. Hatakeyama H, Akita H, Harashima H. The polyethyleneglycol dilemma: advantage and disadvantage of PEGylation of liposomes for systemic genes and nucleic acids delivery to tumors. Biol Pharm Bull. 2013; 36(6):892–9. [PubMed: 23727912]

41. Verhoef JJF, Anchordoquy TJ. Questioning the use of PEGylation for drug delivery. Drug Deliv Transl Re. 2013; 3(6):499–503.

42. Tiruppathi C, Song W, Bergenfeldt M, Sass P, Malik AB. Gp60 activation mediates albumin transcytosis in endothelial cells by tyrosine kinase-dependent pathway. J Biol Chem. 1997; 272(41):25968–75. [PubMed: 9325331]
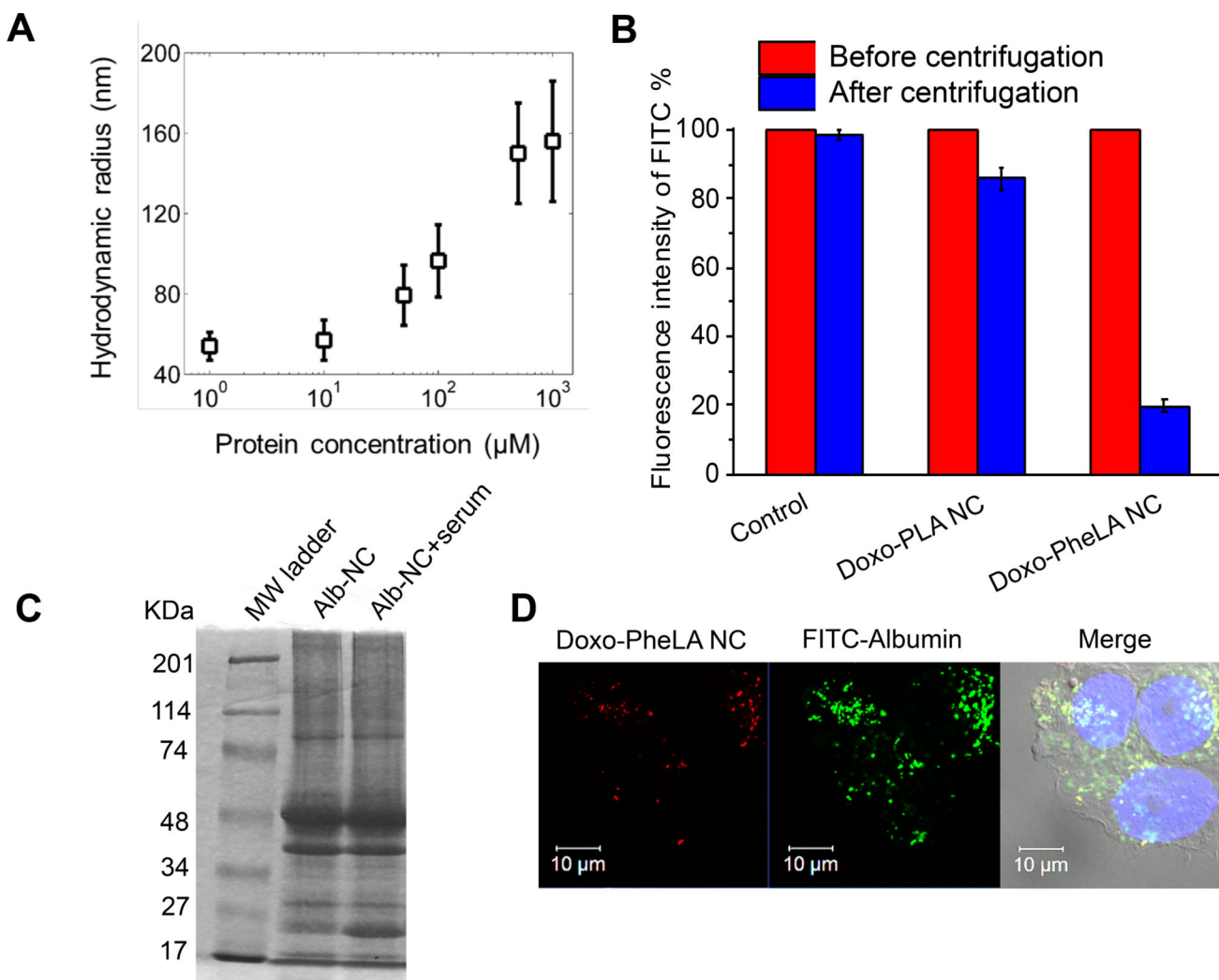
Figure 1.

Characterization of Alb-NCs. (A) Adsorption of human serum albumin onto Doxo-PheLA NCs. Hydrodynamic radius of Alb-NCs plotted as a function of the concentration of albumin. (B) Percentage of fluorescence intensity of FITC-albumin after binding with Doxo-PLA NCs and Doxo-PheLA NCs. (C) Alb-NCs incubated in human serum buffer, then extracted after extensive wash and subjected to SDS–PAGE analysis. The albumin band was shown between 48kDa and 74kDa. Left column: Alb-NC; Right column 2: Alb-NC + serum (Alb-NCs extracted from human serum buffer (2× dilution with PBS, 10 μL loading)). (D) Co-localization of Doxo-PheLA NCs (red fluorescence) with FITC-albumin (green fluorescence) in MCF-7 cells.
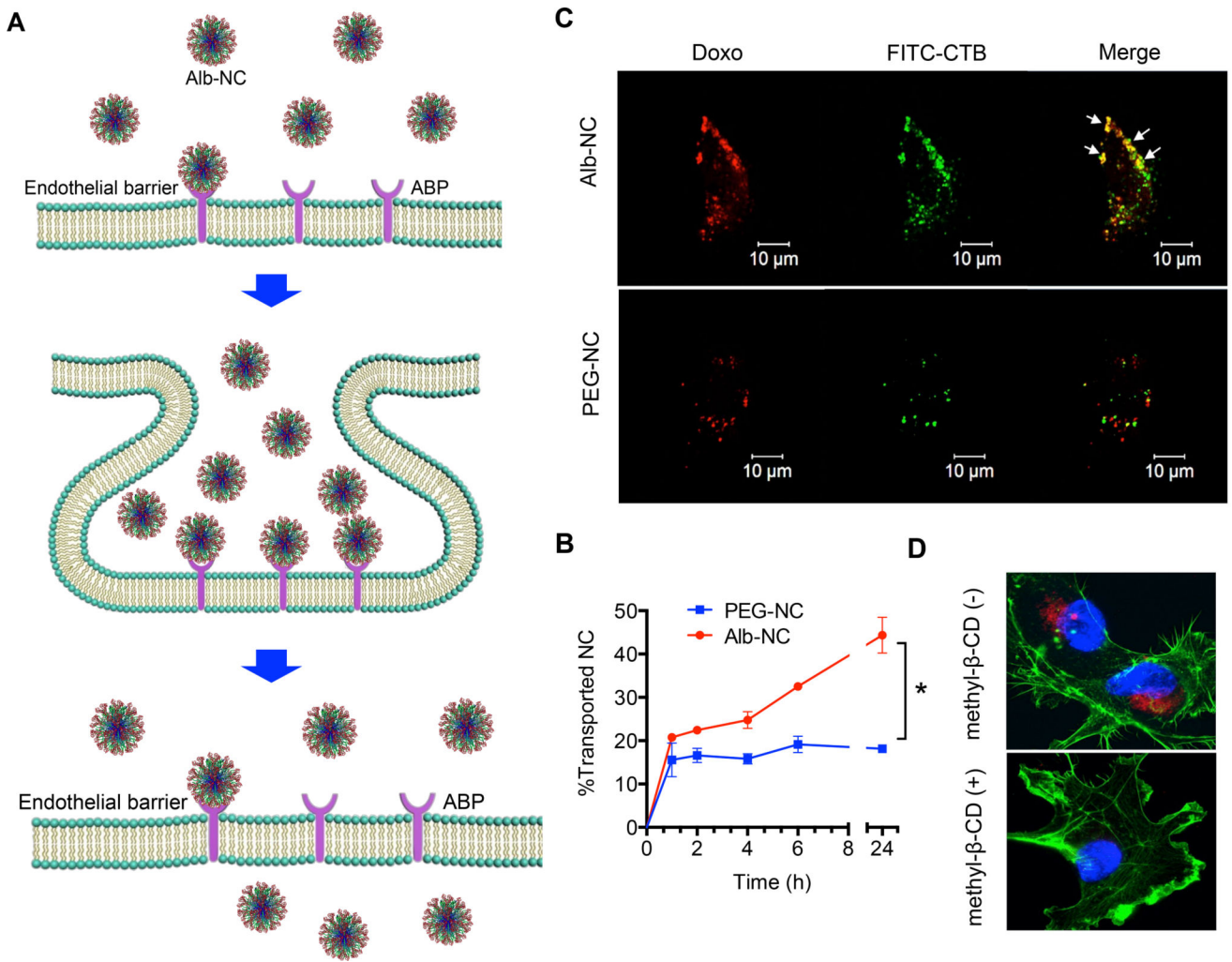
Figure 2.
Albumin induces the transendothelial transport of NCs via caveolae-mediated pathway. (A) Schematic illustration of binding of Alb-NCs to endothelial plasmalemma in caveolae by ABP (e.g., gp 60) and subsequent formation of the caveolae vesicle to facilitate transcytosis of NCs across endothelial cell barrier to reach tumor interstitium. (B) Transcytosis kinetics of Alb-NCs and PEG-NCs across the HUVEC monolayer. (C) Confocal images of Alb-NCs (red, upper panel) and PEG-NCs (red, bottom panel) and CTB (green) in HUVEC cells are shown. Co-localization of NC staining and FITC-CTB are marked in the merged images (right). (D) Cyclodextrin prevents albumin-induced endocytosis of NCs, analyzed by Zeiss LSM 700 confocal microscopy. Alb-NCs was loaded with Doxo (red). The nucleus was stained with DAPI (blue), and the cell skeleton was stained with Alexa Fluor® 488 Phalloidin (green).
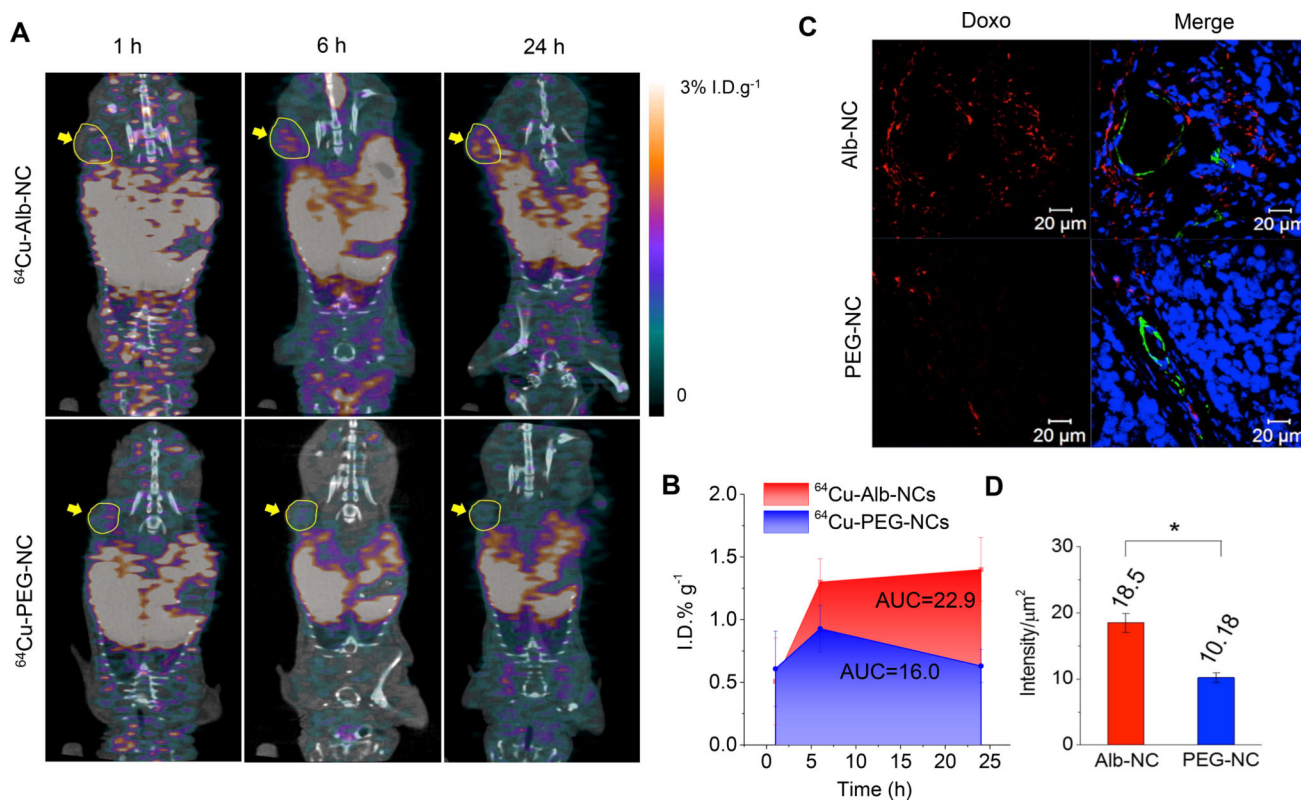
Figure 3.

In vivo tumor accumulation and penetration studies. (A) *In vivo* whole-body dynamic PET/CT imaging of mice treated with ^{64}Cu-Alb-NCs (upper) and ^{64}Cu-PEG-NCs (bottom). Images were taken at 1, 6 and 24 h post intravenous injection of ^{64}Cu-Alb-NCs and ^{64}Cu-PEG-NCs, respectively. The tumor areas were indicated by yellow circle and arrows. (B) Kinetics of the accumulation of ^{64}Cu-Alb-NCs and ^{64}Cu-PEG-NCs in the tumors from 1 to 24 h (average ± SD; n = 3). The AUC was calculated by the trapezoidal rule up to 24 h. (C) Athymic nude mice bearing MCF-7 tumors (size: ~7.0 mm × 8.0 mm) were injected with Alb-NC (40 mg Doxo/kg) and PEG-NC (40 mg Doxo/kg) through intravenous injection (n=3). Mice were euthanized and dissected 6 h post injection. Tumor sections were collected and mounted on glass slides. Fluorescence images were taken by confocal microscopy. Representative images showing the perivascular distribution of Alb-NC and PEG-NC (red,) in relation to blood vessels (green) in tissue sections of MCF-7 tumors. (D) Quantification of the accumulation of Alb-NC and PEG-NC in the tumor tissues by the averaging fluorescence intensity per area (μm^2) by Image J.
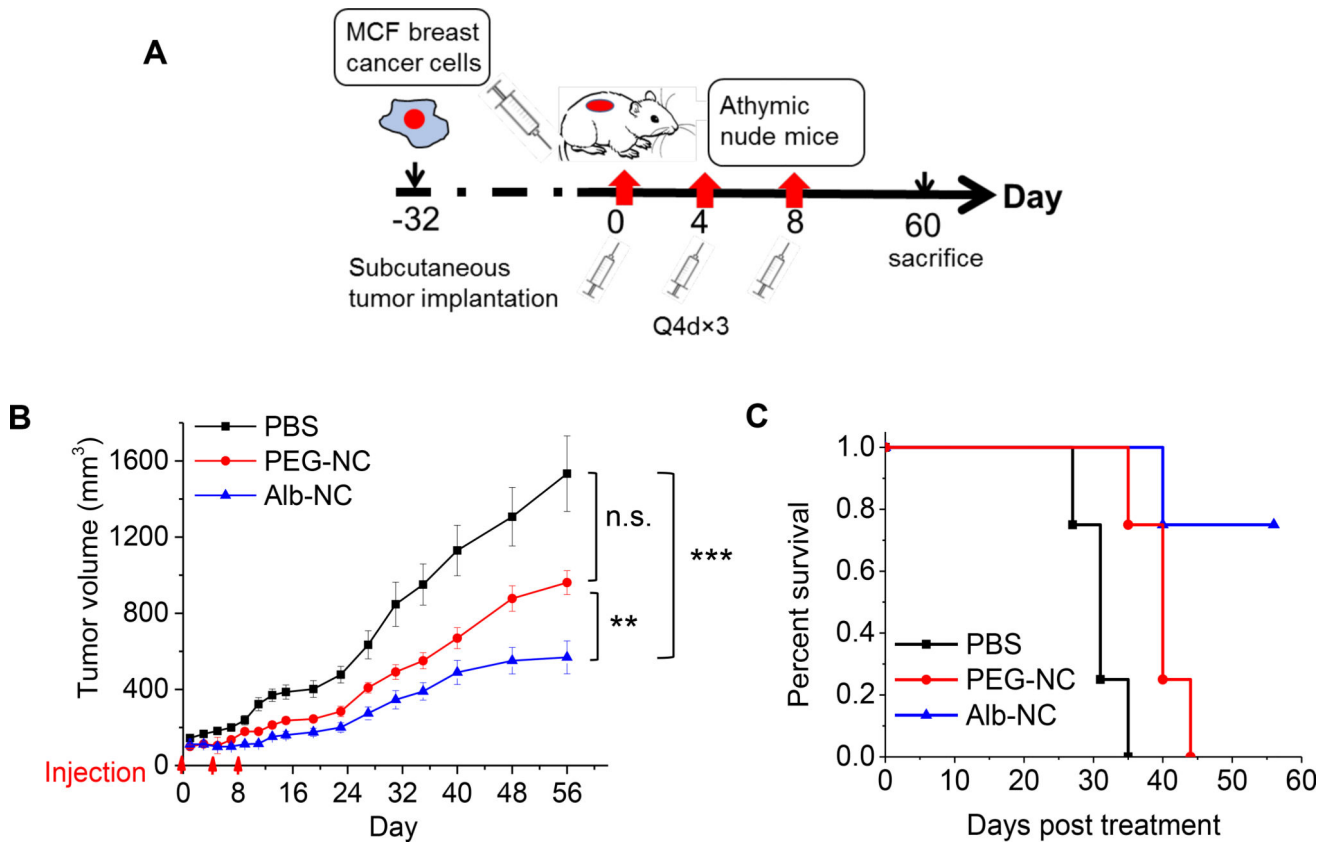
Figure 4.
In vivo antitumor efficacy studies. (A) Schematic timeline of the experimental procedures. (B) MCF-7 tumor growth in athymic nude mice treated with Alb-NCs (40 mg Doxo/kg) and PEG-NCs (40 mg Doxo/kg). PBS was used as negative control. Three doses were administrated on Day 0 and Day 4 and Day 8. All of the data are represented as average ± SEM (n = 16). Unpaired T-Test (two tailed) with Welch's correction was used for statistical analysis. The results were deemed significant at $*p < 0.05$, $** p < 0.01$, $*** p < 0.001$. (C) Kaplan–Meier plots for all groups are shown. Loss of mice was because of treatment-related death, nontreatment-related death, or euthanasia after the end point (900 mm^3) had been reached (n = 4).
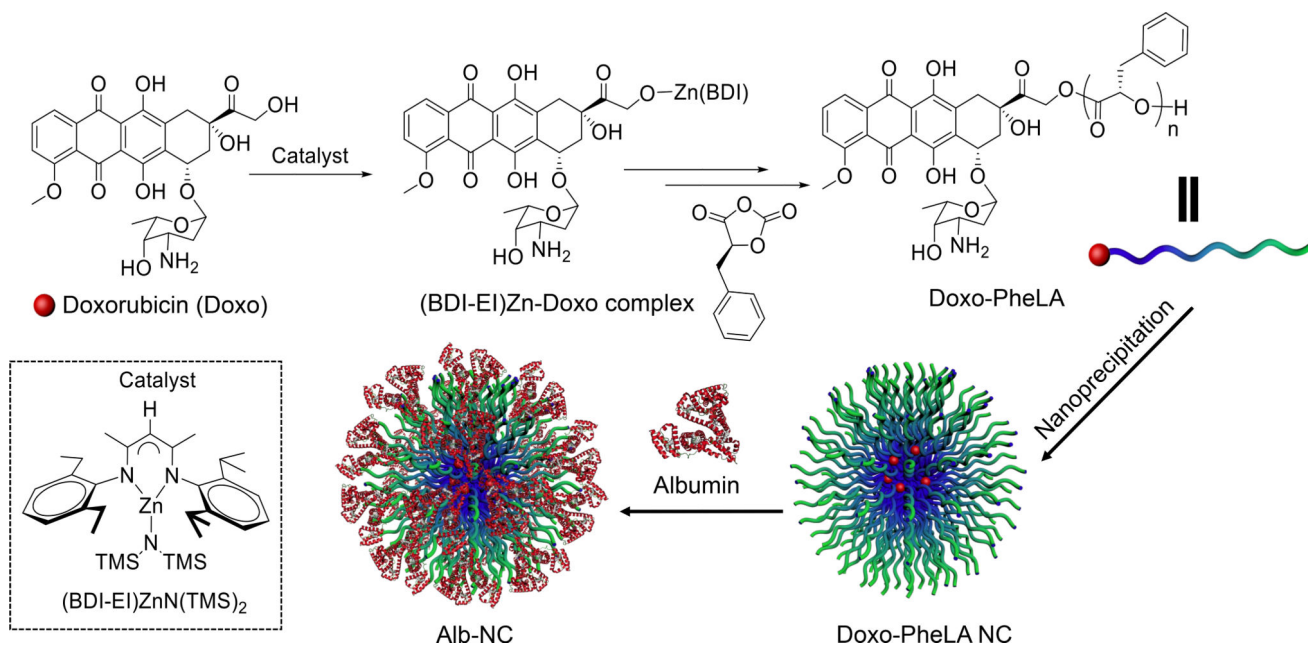
Scheme 1.
Schematic illustration of preparation of Doxo-PheLA conjugates via Doxo-initiated ring opening polymerization of PheOCA and formulation of Alb-NCs.